Article

Not peer-reviewed version

# Tracking Single Mouse Mesenchymal Stromal Cells Migration into Glioblastoma using a Photoconvertible Microcapsules

Olga A Sindeeva *, Polina A Demina, Zhanna V Kozyreva, Daria. A Terentyeva, Olga I Gusliakova, Albert R Muslimov, Gleb B Sukhorukov *

Posted Date: 21 May 2024

doi: 10.20944/preprints202405.1383.v1

Keywords: photoconvertible microcapsules; fluorescent label; surface charge; glioma; human mesenchymal stromal cells; cell migration

*Article*

# Tracking Single Mouse Mesenchymal Stromal Cells Migration into Glioblastoma Using a Photoconvertible Microcapsules

**Olga A. Sindeeva [1,*], Polina A. Demina [2], Zhanna V. Kozyreva [1], Daria A. Terentyeva [1], Olga I. Gusliakova [1,2], Albert R. Muslimov [3] and Gleb B. Sukhorukov [1,4,5,*]**

[1] Vladimir Zelman Center for Neurobiology and Brain Rehabilitation, Skoltech, 3 Nobel Str., 121205 Moscow, Russia; o.sindeeva@skoltech.ru (O.A.S); zhanna.kozyreva@skoltech.ru (Zh.V.K.); daria.terentyeva@skoltech.ru (D.A.T.); o.gusliakova@skoltech.ru (O.I.G.); g.sukhorukov@skoltech.ru (G.B.S.)

[2] Science Medical Center, Saratov State University, 83 Astrakhanskaya Str., 410012 Saratov, Russia; polina.a.demina@list.ru (P.A.D.); olga.gusliakova17@gmail.com (O.I.G.)

[3] Saint Petersburg State Chemical and Pharmaceutical University, 14 Professora Popova Str., lit. A, 197022 St. Petersburg, Russia; albert.r.muslimov@gmail.com (A.R.M.)

[4] Life Improvement by Future Technology (LIFT) Center, 121205 Moscow, Russia; g.sukhorukov@lift.center (G.B.S.)

[5] School of Engineering and Materials Science, Queen Mary University of London, Mile End Road, E1 4NS London, UK; g.sukhorukov@qmul.ac.uk (G.B.S.)

* Correspondence: o.sindeeva@skoltech.ru (O.A.S.); g.sukhorukov@qmul.ac.uk (G.B.S.)

**Abstract:** To elucidate mesenchymal stromal cells (MSC)-tumor intricate and ambiguous interactions, the reliable cell labeling and tracking techniques are imperative. Traditional methods of cell labelling have limitations mostly relevant to need for genetic modification what demands the exploration for alternative strategies. Here, we propose using fluorescent photoconvertible microcapsules containing Rhodamine B (RhB) to study mMSC migration in brain tumors. These 3 μm sized microcapsules are readily internalised by cells and undergo photoconversion under 561 nm laser exposure with fluorescence blue shift on demand. Optimal photoconversion was achieved with a laser irradiation duration of 0.4 ms, which provide a maximal brightness of photoconverted label without an excessive laser exposure on cells. Capsules modified with polyallylamine hydrochloride demonstrated the best potential for intracellular uptake without significantly affecting cell viability, motility, or proliferation. The optimal ratio of 20 capsules per mMSC was determined for labeling. Moreover, migration of individual mMSCs within 2D and 3D glioblastoma cell (EPNT-5) colonies over 2 days and in vivo tumor settings over 7 days was tracked. Our study unveils a robust platform for investigating MSC-tumor dynamics, offering insights into therapeutic strategies. Photoconvertible microcapsules could also become an indispensable tool for studying complex fundamental processes of cell-cell interactions for a wide range of problems in biology and medicine.

**Keywords:** photoconvertible microcapsules; fluorescent label; surface charge; glioma; human mesenchymal stromal cells; cell migration

## 1. Introduction

Mesenchymal stem cells (MSCs), also known as "mesenchymal stromal cells", are the cornerstone, hope, and fear of modern cancer therapy [1]. According to MSCs' inherent tumor-tropic properties, their use as a "Trojan horse" for more effective delivery of encapsulated drug forms into tumors has been proposed [2–6]. Nevertheless, a growing number of oncology studies have demonstrated that MSCs possess dual characteristics related to cancer development. They have been shown to initially reduce the accumulation of reactive oxygen species (ROS) and DNA damage in the

 doi:10.20944/preprints202405.1383.v1



early stages, providing a tumor-suppressive effect. Yet, in later stages, MSCs manifest themselves as tumor promoters, stimulating epithelial-mesenchymal transition and metastasis [7].

Growing controversy regarding the utility of MSCs in cancer therapy requires detailed *in vitro* and *in vivo* studies of their interactions with tumors. In turn, such studies require reliable approaches to mark and track the cells of interest [8]. This task is particularly challenging for long-term studies or monitoring of individual cells (e.g., the cell that is better at producing specific substances) in heterogeneous populations [9]. Photoswitchable and photoconvertible proteins [10] and dyes [11,12] partially address these challenges. They enable tracking of the entire pool of cells *in vitro* and *in vivo*, as well as the identification and labeling of individual cells of interest using local laser action [11,13,14]. Nevertheless, the use of photoswitchable or photoconvertible proteins requires transfection of the selected cell line [13,15], which may not be safe for further use of the MSCs population under study in therapy. Additionally, this may also be a limitation if the studied population has already been transfected and produces any protein, including fluorescent ones. Photoconvertible dyes are typically highly lipophilic and partition stably but non-covalently into cell membranes [12]. Such dyes tend to transfer to the membranes of nearby cells in close contact [16], potentially distorting research results. It should also be noted that tracking dye fluorescence is typically $10^2$ - $10^3$ times brighter than antibody fluorescence [8]. Therefore, it is extremely difficult to establish conditions where the presence of tracking dye or label does not compromise the ability to detect other probes being used. Furthermore, both proteins and dyes tend to be dilute the label over time due to cell division. This ultimately leads to the inability to detect the photoconverted cell over time, sometimes within just a few hours [17,18]). Additionally, in the case of individual labeling of several cells, neither approach can distinguish one labeled cell from another, hindering the ability to trace the fate of each of them separately.

Previously, we proposed the concept of using thermally treated polymer photoconvertible capsules containing Rhodamine B (RhB) for labeling and tracking individual cells [19–21]. These capsules can be internalized by cells and irreversibly photoconverted inside of them using localized laser exposure. Subsequently, the synthesis technique was improved, significantly increasing the number of capsules in the sample (250 times) due to heat treatment in a polyvinyl alcohol gel environment [22]. In this work, a number of dyes capable of photoconversion after encapsulation during hydrothermal synthesis were also selected and described. Apperantly, RhB emerged as the most promising and stable dye. The promise and safety of labeling have been demonstrated across a wide range of cell lines, including fibroblasts, macrophages, myoblasts, cancer cell lines [19], and even human MSCs [23]. These studies have revealed significant differences in the number of microcapsules required for labeling, emphasizing the need for careful selection for each specific line. Nevertheless, several issues remain unresolved, including (I) the possibility of enhancing the efficiency of microcapsule uptake by modifying their surface; (II) assessing the brightness limits of microcapsules depending on laser exposure parameters; (III) tracking cells labeled with microcapsules in other cell line colonies; (IV) evaluating the possibility of using the developed approach for *in vivo* cell detection.

In this study, fluorescent photoconvertible microcapsules containing RhB with surface modification using positively and negatively charged polyelectrolytes were explored and tested. The limits of microcapsule photoconversion efficiency depending on the duration of exposure to a 561 nm laser were estimated. Furthermore, the influence of capsule number (with different surface charges) on the viability, internalization efficiency, proliferation, and mobility of mMSCs was assessed. Finally, the migration of individual mMSCs within 2D and 3D EPNT-5 glioblastoma cell colonies and tumor *in vivo* was studied using photoconvertible microcapsules.

## 2. Materials and Methods

### *2.1. Materials*

Poly(4-styrene sulfonate) sodium salt (PSS, Mw = 70 kDa), poly(allylamine hydrochloride) (PAH, Mw = 17.5 kDa), dextran sulfate sodium salt (DS, Mw = 40 kDa), ethylenediaminetetraacetic

 doi:10.20944/preprints202405.1383.v1



acid disodium salt (EDTA), calcium chloride dihydrate, sodium carbonate, Evans Blue, and Rhodamine B were purchased from Sigma-Aldrich (Taufkirchen, Germany). Dimethyl sulfoxide (DMSO) was obtained from Merck (Darmstadt, Germany). DiIC18(5) (DiD) lipophilic tracer was obtained from Lumiprobe (Moscow, Russia). Polyvinyl alcohol (PVA) powder (Mw = 72,000 g/mol with a degree of hydrolysis of 85-89%), MTT (thiazolyl blue tetrazolium bromide, more than 98%) was supplied by AppliChem GmbH (Darmstadt, Germany). All the chemicals were used without further purification. Deionized water with specific resistivity higher than 18.2 MΩ·cm produced from the Milli-Q® Direct 8 water treatment system (Merck Millipore, Darmstadt, Germany) was used to prepare all solutions. Calcein-AM fluorescent dye and Hoechst 33258 were purchased from Thermo Fisher Scientific (OR, USA). Dulbecco's Phosphate Buffered Saline (DPBS) without calcium and magnesium, trypsin/EDTA solution, penicillin/streptomycin solution, Dulbecco's Modified Eagle Medium F12 (DMEM/F12), Eagle's Minimum Essential Medium (EMEM) and Fetal Bovine Serum (FBS) was supplied by Wuhan Servicebio Technology Co., Ltd (Wuhan, China).

### *2.2. Synthesis and Characterization of Photoconvertible Microcapsules*

Synthesis of photoconvertible polymer microcapsules was done according to a previously described procedure [22]. Initially, vaterite cores were prepared by mixing calcium chloride dihydrate and sodium carbonate salts (1 M, 0.650 μL) in 3 mL of water. Then, polyelectrolyte layers were deposited by alternating PAH and PSS (1 mg/mL in 0.15 M NaCl). Each layer was adsorbed for 10 minutes at the rotator. After each cycle, the sample was washed three times with water via centrifugation. Upon achieving $(PAH/PSS)_4$ layers, the vaterite cores were dissolved in a 0.2 M EDTA solution. Then, the sample was immersed in a DS aqueous solution (2 mg/mL) for 1 hour at the rotator. After additional washing via centrifugation, the capsules were combined with RhB solution (0.5 μg/mL) and PVA gel (final PVA gel concentration was 15%). The prepared mixture was placed in the autoclave and exposed to 3-hour thermal treatment at 180 °C. Final microcapsules underwent thorough water rinses to remove PVA gel and excess RhB dye. They were additionally modified by applying PAH and PSS polymers to form samples with PAH and PAH/PSS outer layers.

Capsules after hydrothermal treatment were examined using a scanning electron microscope (SEM) VEGA III (TESCAN, Brno, Czech Republic). Capsule suspension was deposited on a silicon wafer to dry completely. Subsequently, a thin gold film (~5 nm thickness) was applied via a rotary-pumped coater. ImageJ software was used for analysis of SEM images [https://imagej.net/ij/index.html].

### *2.3. Photoconversion and Imaging of Microcapsules Using a Confocal Microscope*

A confocal laser scanning microscope (CLSM) Leica TCS SP8 X (Leica, Germany) equipped with 20x\0.70 NA air objective and several discrete lasers was used for capsule visualization and photoconversion. For microcapsule excitation, a 561 nm laser was used with an emission range of 580–620 nm (red channel). For photoconverted capsules, a 488 nm laser was used with an emission range of 505–540 nm (green channel). The DiD fluorescent dye was excited with the 671 nm laser, and the emission range was 740–790 nm.

The photoconversion of fluorescent microcapsules was carried out with a 561 nm laser of the CLSM system. The laser power density (LPD) was 451 kW/cm$^2$, the scanning speed was 10 Hz, and the scanning area was 12.11 × 12.11 μm. Gwyddion v.2.63 software was used to measure the angularly averaged fluorescence intensity of capsules before and after photoconversion.

### *2.4. Cell Experiments*

#### 2.4.1. Isolation of mMSCs

Bone marrow derived MSCs from the C57BL/6- Tg(ACTbEGF)1Osb/J mouse (Jackson Labs, United States) that express green fluorescent protein (GFP) were isolated using using a modified technique developed by Professor Popov [24]. After euthanasia by the cervical dislocation method bone marrow from the tibia and femur was washed with a syringe using growth medium

 doi:10.20944/preprints202405.1383.v1



(DMEM/F12 with 10% fetal calf serum). Cells were washed twice with 10 mL of DPBS, centrifuged at 300G for 5 min, and suspended in 50 ml complete growth medium. Cell suspensions were placed in six-well plates at 5 × $10^6$ cells/ml density in 4 mL per well. Confluent primary cultures were washed twice with DPBS and treated with Trypsin (0.25%) and EDTA (1 mM) solution to detach cells from the surface. After that cells were suspended in the complete growth medium and cultivated for further experiments.

2.4.2. Cultivation of mMSCs and EPNT-5 Cells

EPNT-5 (mouse glioblastoma) cells were obtained from the Russian Cell Culture Collection of Vertebrates, Institute of Cytology, St. Petersburg, Russia. Stock vials of frozen mMSCs and EPNT-5 cells (1 mL) were thawed using a water bath (37 °C). Then, the cell suspension was transferred to 5 mL of warm (37 °C) DMEM/F12 (for mMSCs) or EMEM (for EPNT-5) growth medium (10% FBS, 1% penicillin/streptomycin), centrifuged (3 min, 1000 RPM), and placed on flasks in fresh growth medium for subsequent cultivation (37 °C, humidified atmosphere with 5% $CO_2$). The medium was refreshed 24 h after defrosting. For routine maintenance of culture (passage), cells are seeded at a confluence of approximately 15-20% and grown to a confluence of approximately 80%. For passage, mMSCs and EPNT-5 cells were detached with trypsin/EDTA solution for 5 min.

2.4.3. Viability Investigation on mMSCs (MTT Test)

*mMSCs* were plated on a 96-well plate at the amount of 5 × $10^3$ cells per well and incubated for 12 h (37 °C, humidified atmosphere with 5% $CO_2$). Then, 1, 5, 10, 15, 20, and 25 microcapsules per cell were added in 100 μL of fresh DMEM/F12 growth medium to the wells (in 6 repetitions). *mMSCs* without microcapsules were used as a positive control. After 24 and 48 h of incubation, the culture medium was replaced with 100 μL of fresh medium containing 10% MTT stock solution (5 mg/mL in DPBS buffer) and incubated for 3 h at 37 °C. Then, the culture medium with MTT reagent was carefully removed, and 100 μL of DMSO solution was added to each well and incubated for 15 min using a thermoshaker (TS-100 Biosan) at 37 °C and 300 RPM to dissolve the formazan crystals. The absorbance of each well was measured at 570 nm wavelength using a spectrophotometer ClarioSTAR Plus (BMG Labtech, Ortenberg, Germany).

2.4.4. Influence of Microcapsule Amount on Internalization Efficiency and mMSCs Proliferation

*mMSCs* were plated on a 12-well plate at the amount of 6 × $10^4$ cells per well and incubated for 12 h under identical conditions. Next, 15, 20, and 25 capsules per cell were added to the wells (in 3 repetitions) in 1 mL of fresh growth medium and incubated for 24 h to allow internalization. Then, the culture medium was removed, and the cells were carefully washed three times with DPBS to remove uncaptured capsules. Next, the cells were stained using 150 μL of stock solution with Calcein-AM and Hoechst 33258 in a serum-free medium which was added to each well and incubated for 20 min. After staining, the cells were washed with a DPBS buffer. Fluorescence images were obtained from 3 randomly selected fields for each well to compare cell proliferation with and without microcapsules. Proliferation was calculated by the number of *mMSCs* cell nuclei (stained by Hoechst 33258) per 1 $cm^2$. Images were obtained using inverted microscope Olympus IX73 (Olympus, Tokyo, Japan) equipped with 20x/0.40 NA objective (Olympus), U-HGLGPS light guide-coupled illumination system (Olympus), and a monochrome camera to capture fluorescent images with standard wavelength filters (Ex1 = 360-370 nm, Em1 = 420-460 nm, Ex2 = 470-495 nm, Em2 = 510-550 nm, Ex3 = 540-550 nm, Em3 = 575-625 nm).

Then, 150 μL trypsin/EDTA solution was used to harvest the cells, which were then centrifuged (3 min, 1000 RPM) while adding the equivalent quantity of complete growth medium. Next, the medium with trypsin was removed, and cells were suspended in fresh DPBS supplemented with 2% FBS and measured using an ImageStream X Mark II Imaging flow cytometer (Luminex, USA). The measurement was performed using INSPIRE software with the following equipment settings: 40×magnification, low flow rate/high sensitivity, 405 nm with a laser power of 10 mW, and 488 nm

 doi:10.20944/preprints202405.1383.v1



laser at 5 mW. Internalization investigations for *mMSCs* involved the analysis of 10,000 objects per sample. The number of internalized capsules was calculated using the Spot Count feature of the IDEAS software (Luminex, USA). The presence of an object visualization system in the cytometer also made it possible to analyze the data taking into account the number of capsules internalized by the cells.

2.4.5. Influence of Microcapsules on mMSCs Movement (Scratch Test)

*mMSCs* cells were plated in a 24-well plate at a density of $3 \times 10^4$ cells/well and then incubated for 12 h. After this, microcapsules were then added at concentrations of 15, 20, and 25 capsules per cell and incubated for 24 h. A scratch was made using a pipette tip according to the described protocol [25]. The *mMSCs* were washed three times with DPBS to remove detached cells and non-internalized microcapsules. Next, 1 mL of medium with 2% FBS was added to each well. Cells without capsules under the same conditions served as a negative control. Cells without capsules in a medium supplemented with 10% FBS were selected as a positive control. Fluorescence images of *mMSCs* were obtained after staining with Calcein AM using 4x\0.3 NA objective immediately after the scratch, and 12 and 24 h later. The migration stage was evaluated by calculating the area between the edges of the wound using ImageJ software.

2.4.6. mMSCs Tracking into the EPNT-5 2D and 3D Colony

For mMSCs tracking into 2D EPNT-5 cells colony, 2 well silicone inserts with a defined 500 μm cell-free gap were used. The silicone insert was placed on a μ-Dish 35 mm (Ibidi) with a 500 μm grid for the convenience of monitoring changes in the growth areas of cell colonies and to determine the position of labeled mMSCs. The EPNT-5 cells were stained with 0.1% DiD membrane dye in ethanol (2 μL of the solution was added to 200 μL of the medium for 30 min). Then, EPNT-5 cells and mMSCs (containing microcapsules) were placed in the well of silicone insert ($2 \times 10^3$ cells per well) and incubated for 12 h (5% CO2 at 37 °C). Next, the silicone insert was removed and the migration test was started.

For mMSCs tracking in 3D EPNT-5 cells, the colony used low adhesion 96-well floater plates SDL3D (SPL lifesciences, Korea) to grow spheroids. EPNT-5 (labeled DiD) and mMSCs (containing microcapsules) were mixed in a ratio of 5:1, respectively. Photoconversion of capsules into individual mMSCs and monitoring of their migration in spheroids was carried out after 24 hours.

Area of interest images were obtained using a confocal fluorescence microscope before and 15 min and 24, 48, and 72 h after microcapsule photoconversion. The settings for obtaining images and photoconversion of the microcapsules were similar to those described above. EPNT-5 cells were visualized using a 671 nm laser with a detection range of 685–790 nm.

*2.5. Animal Experiments*

The laboratory animals were treated according to the Geneva Convention of 1985 (International Guiding Principles for Biomedical Research Involving Animals). All experimental procedures were performed on C57BL male mice 8 weeks old using general anesthesia via intraperitoneal injection (Zoletil mixture (40 mg per kg, 50 μL, Virbac SA, Carros, France) and 2% Rometar (10 μL and 10 mg per kg, Spofa, Czech Republic)). The animals were euthanized by an overdose of anesthesia at the end of the experiments.

For implantation of EPNT-5 cells in the mouse brain (orthotopic glioblastoma model) the cut was made over the sagittal crest from the bregma to the lambdoid suture. Then periosteal membrane was removed and a small burr hole without tearing the dura mater. The EPNT-5 cells ($1 \times 10^6$ cells per mouse) were injected at a depth of 1 mm from the brain surface with a Hamilton microsyringe in a volume of 5 μL. Afterward, the burr hole was sealed with sterile bone wax and the wound was sutured. 21 days after implantation EPNT-5 cells, labeled mMSCs ($1 \times 10^6$ cells per mouse) were injected in a similar manner to a depth of 3 mm.

 doi:10.20944/preprints202405.1383.v1



*2.6. Statistical Analysis*

Statistical analysis was performed using GraphPad Prism software. Results were presented as mean ± standard deviation (SD). The difference between control and experimental groups was analyzed by using one way-ANOVA with a post-hoc Tukey HSD test. P values less than 0.05 were considered statistically significant.

## 3. Results and Discussion

*3.1. Synthesis and Characterization of Polyelectrolyte Fluorescent Microcapsules*

Polymer microcapsules containing RhB were synthesized according to the procedure described earlier [22,23]. On their base, three types of capsules were prepared with some modifications (Figure 1A). Sample 1 is regular capsules thermally treated in PVA gel with RhB. Sample 2 and sample 3 are capsules additionally covered with layers of PAH and PAH/PSS, respectively. For convenience, samples were named according to the outer layer of the capsules: PVA, PAH, and PSS.

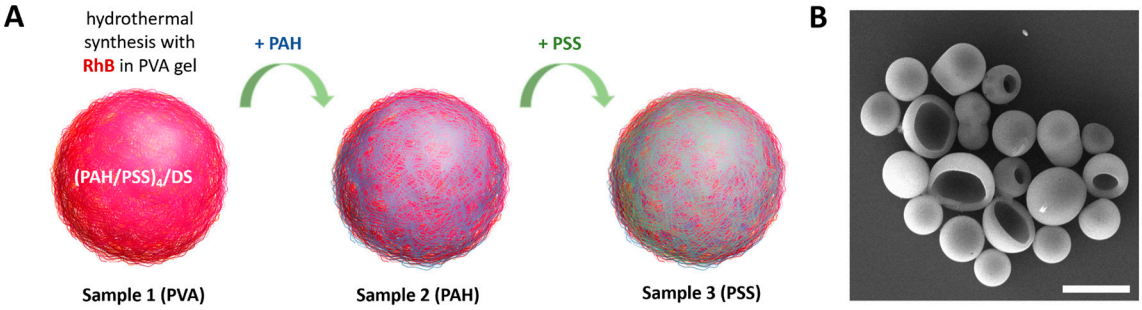


**Figure 1.** (A) General scheme for the synthesis of photoconvertible polyelectrolyte microcapsule samples with various surface modifications. (B) Typical SEM images of polyelectrolyte microcapsules after hydrothermal synthesis with RhB in PVA gel. Scale bar - 5 μm.

A typical SEM image of the PVA capsules is presented in Figure 1B. The morphology of the capsules did not differ between samples of capsules with various surface modification. The modification of the capsule surface also did not lead to an increase in size (Table 1).

**Table 1.** Size and electrokinetic ζ-potential of polyelectrolyte microcapsules based on $(PAH/PSS)_4$ after surface modification.

| Type of microcapsules | Size, μm | ζ-potential, mV |
|---|---|---|
| Thermally treated $(PAH/PSS)_4$ in PVA gel with RhB (*Sample 1 (PVA)*) | 3.3 ± 0.6 | -17.5 ± 1.2 |
| Thermally treated $(PAH/PSS)_4$ in PVA gel with RhB, covered with PAH (*Sample 2 (PAH)*) | 3.4 ± 0.7 | -7.6 ± 0.6 |
| Thermally treated $(PAH/PSS)_4$ in PVA gel with RhB, covered with PAH/PSS (*Sample 3 (PSS)*) | 3.3 ± 0.8 | -18.6 ± 2.6 |

The ζ-potential of three samples is listed in Table 1. PVA and PSS capsules had a negative charge of around -18 mV and an outer layer of cationic PAH increased the charge of capsules to -7.6 mV. PAH is a weak polyelectrolyte that is pH-dependent, so it can not always completely compensate for the negative charge of capsules to positive values [26].

*3.2. Selection of Optimal Photoconversion Parameters Using Confocal Microscope*

For stable cell labeling and tracking it is important to select photoconversion parameters that provide a maximal bright fluorescence of the labels after the laser irradiation. In previous work [23], the laser power density (LPD), included in the scanning electron microscope, was chosen to be 451

 doi:10.20944/preprints202405.1383.v1



kW/cm² as suitable for photoconversion. Nevertheless, there is still the need to choose optimal irradiation duration which provides a bright photoconverted label and does not cause an excessive laser exposure. This can be critical in cell experiments to avoid unnecessary cell death.

CLSM of three samples of capsules PVA capsules and those modified with PAH and PSS polymers are presented in Figure 2A. Here, photoconversion of capsules was performed using the same LPD but changing the duration of one-pixel irradiation from 0.2 to 0.6 ms. According to the obtained images, capsules retained their photoconversion properties after the addition of extra polymer layers. Thus, surface modification did not affect the possibility to photoconvert capsules. Indeed, the usual double thickness of the capsule shell prepared by the LbL approach is about 50 nm in the case of six bilayers [26]. It means that a single or double additional polyelectrolyte layer is even thinner, which is not an obstacle for the confocal laser.

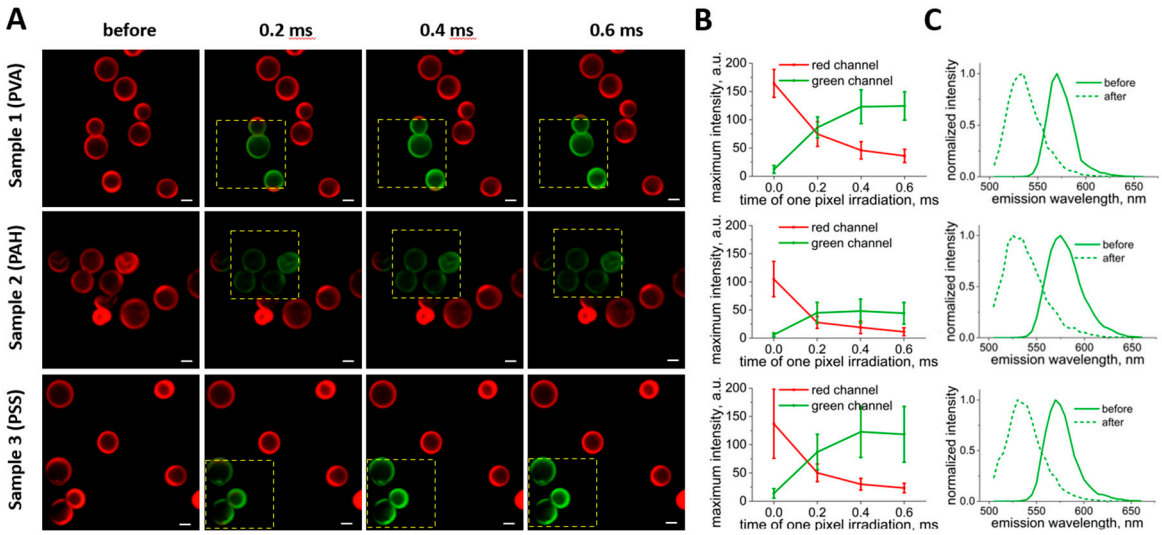


**Figure 2.** (A) Photoconversion of microcapsules using 561 nm laser depending on the duration of one pixel irradiation. Laser exposure area marked with yellow square (size - 1024 × 1024 pixels (12.11 × 12.11 μm)). Excitation – 488 nm, emission: 505 – 540 nm (green channel), excitation – 561 nm, emission: 580–620 nm (red channel). Scale bar – 2μm. (B) Changes in capsules maximum fluorescence intensity in green and red channels depending on the duration of one pixel irradiation. (C) $\lambda$-scans before and after photoconversion at 0.4 ms one pixel irradiation duration. Excitation – 488 nm.

The change in fluorescence intensity of capsules after each irradiation step in green and red channels is presented in Figure 2B. The intensities were calculated from changes in capsules angularly averaged fluorescence intensity profiles depending on the duration of one pixel irradiation (Figure A1). It should be noted that the intensity of the signal in the green channel grows reaching the plateau at around 0.4 ms. In the red channel, the intensity decreases reaching close to minimum values at around 0.4 ms as well. Therefore, further irradiation is not required to provide the highest fluorescence signal of photoconverted capsules. Moreover, $\lambda$-scans of capsules (Figure 2C) demonstrated a blue shift of capsules' spectra. It gave the opportunity to detect capsules in different ranges and was also reported previously [19,22]. Therefore, the optimal parameters of photoconversion of capsules containing RhB using a 561 nm laser are LPD 451 kW/cm² and a one pixel irradiation duration of 0.4 ms.

### *3.3. Selection of the Optimal Ratio of Capsules per Cell for Effective and Safe Labeling of mMSCs*

The correctly selected ratio of capsules per cell is of fundamental importance for the successful internalization of capsules into the cytoplasm in sufficient quantities without harm to their morphofunctional state. It is worth noting that the optimal ratio to ensure effective and safe labeling varies significantly among different cell types [19], so it must be carefully selected in each specific

 doi:10.20944/preprints202405.1383.v1



case. In this regard, at the first stage of cell experiments, the viability of mMSCs was assessed by metabolic activity at 24 and 48 h after adding 0, 1, 5, 10, 15, 20, and 25 capsules per cell.

Samples 1 (PVA) and 3 (PSS) did not have a statistically significant cytotoxic effect at all studied ratios of capsules per cell either 24 or 48 h after their addition (compared to the control) (Figure 3A). In contrast, the addition of sample 2 (PAH) was accompanied by a statistically significant decrease in metabolic activity even when adding 5 capsules (after 24 hours) and 1 capsule (after 48 hours) per cell. For this sample, a smooth trend of decreasing metabolic activity was found depending on the number of microcapsules added after both 24 and 48 h. It is important to note, that even the highest ratios tested (15, 20, and 25 capsules per cell) did not reduce metabolic activity by more than 30 %. The difference in mMSCs metabolic activity after the addition of 15 and 25 capsules per cell also did not exceed 6 % at the studied time points. Therefore, the internalization efficiency of different types of capsules at these concentrations was assessed in detail.

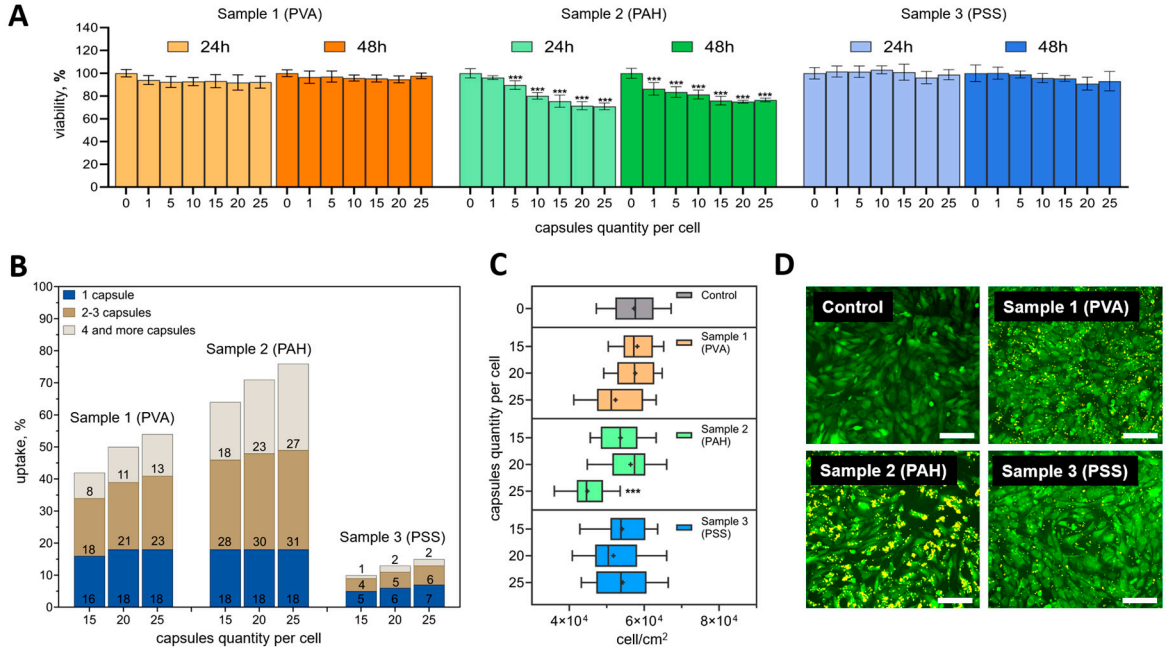


**Figure 3.** (A) Dependence of metabolic activity of mMSCs on the number of added polyelectrolyte microcapsules with various surface modifications. Data is presented as mean ± SD, ***P < 0.001. (B) Dependence of the percentage of cells in the population that internalized the microcapsules with various surface modifications 24 h after incubation with different concentrations. (C) The influence of the microcapsules amount on mMSCs cell proliferation at different initial cell densities 24 h after incubation. Data is presented as mean ± SD, ***P < 0.001. (D) Fluorescence images of mMSCs 24 h after cultivation with 25 capsules per cell (cell cytoplasm stained with Calcein AM (green) and microcapsules – Rhodamine B (yellow)). The scale bar is 200 μm.

As expected, internalization efficiency increased with an increasing number of capsules per cell (Figure 3B). A common tendency for all types of capsules was also observed to increase the proportion of cells capturing 2-3 or more than 4 capsules. The percentage of cells that captured only 1 capsule was not significantly different. It is noteworthy that sample 2 (PAH) was internalized better than the rest of the samples. The efficiency of its internalization was 63.5 ± 6.4, 71 ± 2.8, and 75.9 ± 0.9 % for the ratios of 15, 20 and 25 capsules per cell, respectively. Sample 1 (PVA) was internalized by mMSCs less efficiently – 42.1 ± 5.1, 49.8 ± 1.7, and 54.5 ± 4.5 %, respectively. The least promising was sample 3 (PSS). For this type of capsule, the internalization efficiency did not exceed 7.3 ± 0.2 % at the highest capsule concentration.

 doi:10.20944/preprints202405.1383.v1



The addition of PVA and PSS-modified capsules did not have a notable effect on mMSC proliferation at all concentrations tested (Figure 3C). Significant differences in proliferation were only found when PAH-modified capsules were added at a rate of 25 capsules per cell.

The difference in the interaction of different types of capsules with cells was especially clearly visible in fluorescent images 24 h after incubation (Figure 3D). Capsules that were not internalized and did not interact with the cell membrane were removed during washing. The images were fully correlated with the internalization data obtained by flow cytometry. PAH-modified capsules densely covered the mMSCs membrane, while PSS-modified capsules were visualized as single objects.

This effect may be due to the fact that the cell membrane has a negative charge, therefore, more positively charged capsules (like PAH-modified capsules) are attached to cells faster and stronger than negatively charged, which was reported previously [27]. At the same time, that particles reported to have positive charge resulting on pronounced cytotoxic effect [28], which is fully consistent with the presented data (Figure 3A). Capsules and other micro and nanocontainers with a pronounced negative charge (like PSS-modified capsules) are usually used for delivery through the bloodstream precisely due to low adhesion to the cell membranes [29], and as a result of a longer circulation time [30]. It is interesting that even despite the slight difference between the samples PSS and PVA in electrokinetic ζ-potential (Table 1), the difference in the effectiveness of internalization was pronounced to a significant extent (Figure 3B).

Analysis of the mMSCs motility using a scratch test revealed only a small statistically significant difference compared to the negative control for a sample of microcapsules modified with PSS at the addition of 25 capsules per cell at 12 h (Figure 4). This difference leveled out at the 24-hour mark. This generally indicates the absence of a significant effect of all selected types and concentrations of capsules on cell mobility.

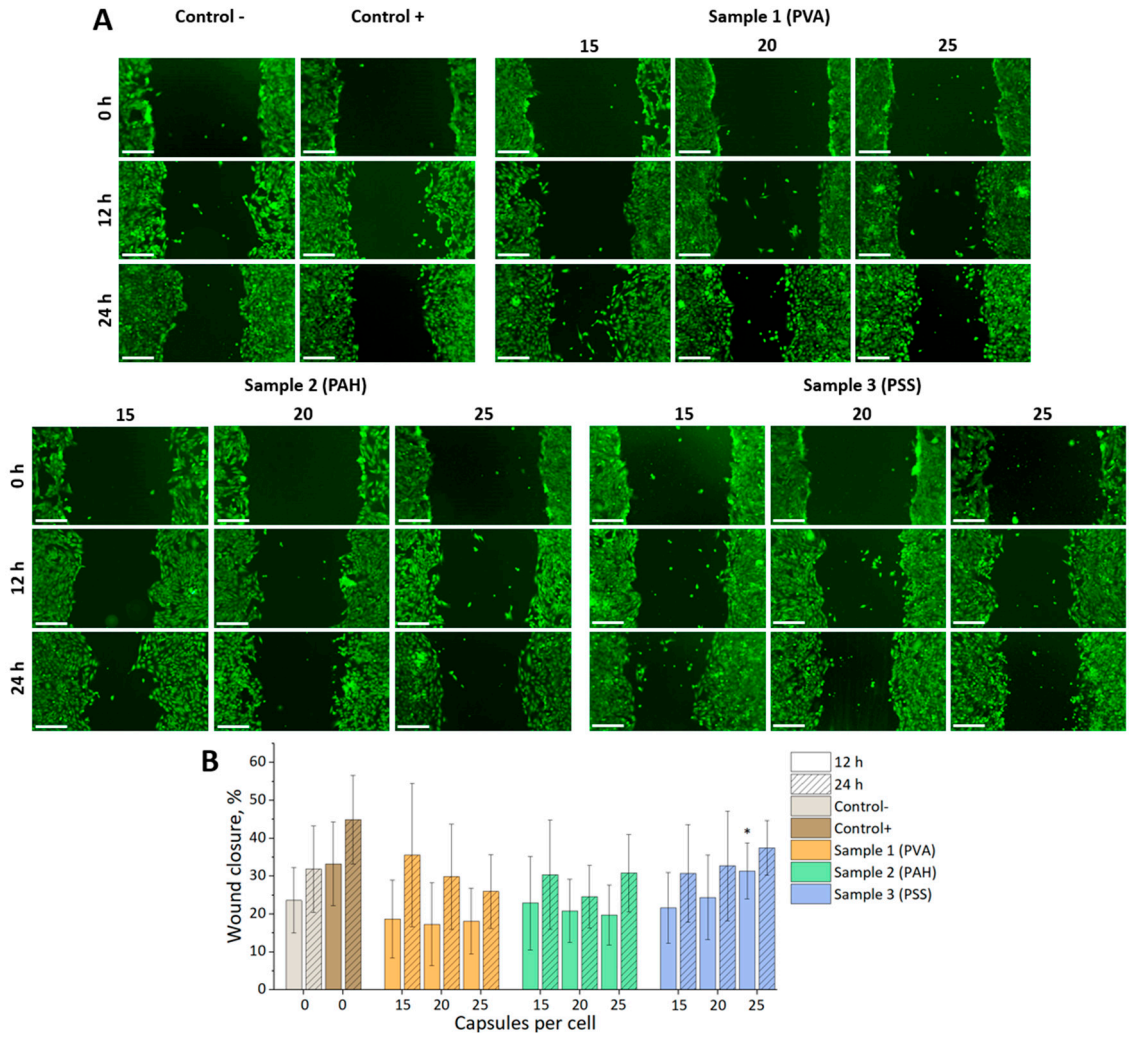

 doi:10.20944/preprints202405.1383.v1



**Figure 4.** (A) Fluorescence images of the wound closure for mMSCs at 0, 12, and 24 h after cultivation with different concentrations of photoconvertible microcapsules (cell cytoplasm stained with Calcein AM (green)). The scale bar is 500 μm. (B) Graph of wound closure over time for mMSCs. *P < 0.05.

The identified trend showed the greatest promise of using PAH-modified capsules for mMSCs labeling in a ratio of 20 capsules per cell. Under these conditions, optimal internalization efficiency was achieved without significantly affecting metabolic activity, cell motility, and proliferation.

*3.4. Tracking the Migration of Individual mMSCs Labeled Using Photoconverted Microcapsules in 2D u 3D EPNT-5 Glioblastoma Cells Colony*

At the next stage of cell experiments, the possibility of monitoring mMSCs migration into glioblastoma cells (EPNT-5) colonies was studied during joint co-cultivation. For this, the mMSCs (labeled with GFP) and microcapsules) and EPNT-5 (labeled with DiD) were placed into 2 wells of silicone inserts with a defined cell-free gap (500 μm). The silicone insert was placed on a μ-Dish 35 mm (Ibidi) with a 500 μm grid for the convenience of monitoring changes in growth areas of cell colonies and determining the position of labeled cells. After 12 h of incubation (5% CO2 at 37 °C), the silicone insert was removed (Figure 5). Note that mMSCs cells were placed into the well 24 h after internalization of the microcapsules (20 capsules per cell) and they had a normal adhesion and morphology despite the presence of capsules inside. Monitoring of the cell migration continued for the next 72 h until the colonies completely merged. Notably, the merge of colonies was accompanied by the beginning of the process of DiD label transferring onto the mMSCs membrane, which made further monitoring of migration difficult. Simultaneously, the capsules localized inside of mMSCs were an additional marker that allowed to identify them reliably. As expected, it was the mMSCs that actively migrated to the glioblastoma colonies, while the EPNT-5 cells did not change their localization. Moreover, the active movement toward the colony of cancer cells began only after 24 hours.

Two cells at the border of the mMSCs colony were laser-labeled at the beginning of the experiment (Figure 5). Labeled and their daughter cells (4 cells at the 48 h of the experiment) tended to move in the direction of the glioblastoma colony. At the same time, after 2 days of the experiment, tracking labeled cells became difficult. This was probably due to the high confluence of cells in the studied area, the loss of some cells during daily washing with DPBS buffer, and the replacement of the medium.

Note that cell doubling led to the division of converted and non-convertible capsules between daughter cells. This required daily monitoring to record the new color coding that the daughter cells received. At the same time, the initial number of capsules (internalized by the cell and converted) was a natural limitation for tracking daughter cells. This is especially relevant and should be taken into account when tracking cells with a short doubling period (12-24 h). Nevertheless, the bright and stable fluorescence of the photoconverted microcapsules was maintained throughout the entire monitoring period, which was a significant advantage compared to photoconvertible proteins. After photoconversion, new fluorescent proteins are continuously produced by the cell expressing the original color. As a result, significant loss of the photoconverted signal occurs through protein turnover and the photoconverted cells revert back to their original color within 24 hours after photoconversion [17,18,31]. On the contrary, photoconversion of the dye (for example DiR) is permanent (since there is no additional source of unconverted dye into the cell). Once photoconverted, the cell does not reacquire the original fluorescence signal, and the photoconverted signal is passed on to the daughter cells. It was reported that the progeny of a photoconverted cell can be tracked over at least three cell doubling, but the brightness of the signal will decrease by half with each cell doubling [12]. Previous studies monitoring the migration of human MSCs using microcapsules were able to track cells for at least 96 hours, while (unlike photoconvertible dyes) it was possible to identify idividual of the labeled cells, including daughter cells, from other labeled cells [23].

 doi:10.20944/preprints202405.1383.v1



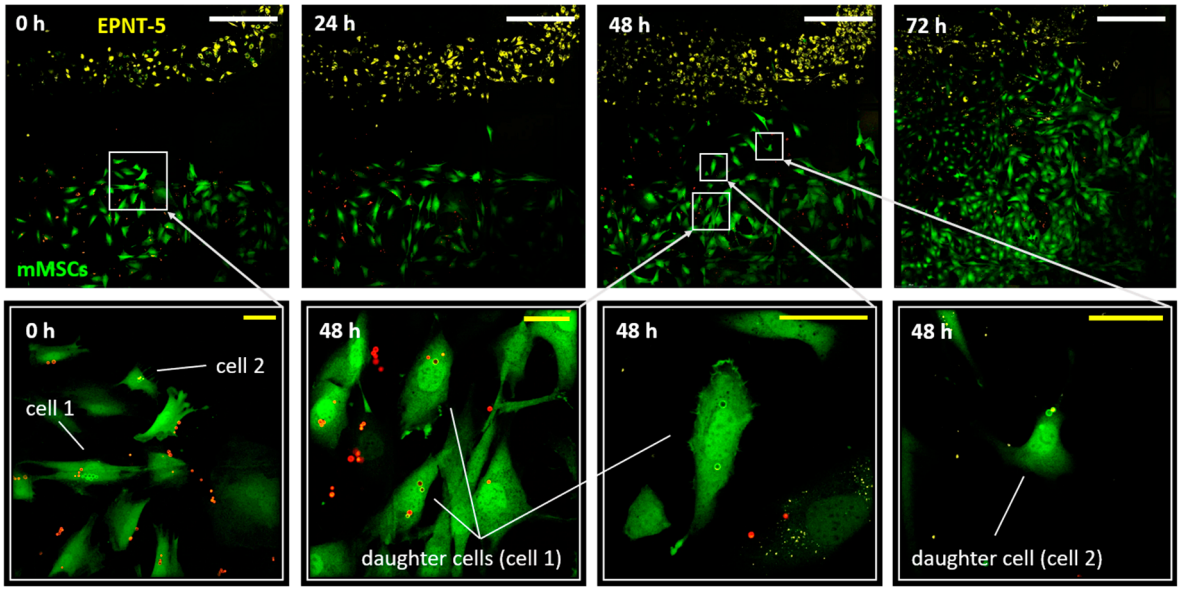


**Figure 5.** Migration of mMSCs (labeled with GFP – green) into a population of EPNT-5 glioblastoma cells (labeled with DiD – yellow) at 0, 24, 48, and 72 h. Cell 1 and Cell 2 were additionally labeled with photoconverted (green) PAH-modified microcapsules. Daughter cells shared converted capsules during doubling. Non-converted capsules – red. White scale bar – 500 μm, yellow – 50 μm. .

To monitor the cells inside the 3D glioblastoma culture, the amount of cells was initially chosen to be at appropriate visualization of all cells in the spheroid (Figure A2) taking into account light penetration. At spheroids made of 600–3000 cells and above we are able to visualize only the outer layer of cells (about 70 μm deep). This made migration monitoring hardly possible in a living spheroid without special optical clearing techniques. In this regard, the number of cells was reduced to 75 with a ratio of mMSCs to EPNT-5 of 1:5, respectively. That parameters made it possible to view all the cells in the spheroid during 3D reconstruction with this number of cells.

Observation of individual labeled mMSCs in the spheroid made identification possible them for at least 48 hours (Figure 6A). 3D reconstruction confirmed the localization of photoconverted capsules in the mMSCs cytoplasm both immediately and 48 h after the experiment started (Figure 6B). At the same time, the continuous growth of the spheroid was observed, which ultimately led to the impossibility of identifying all the cells in it. This experiment also noted the ability of the lipophilic dye DiD to migrate to the mMSCs membrane from EPNT-5 cells membrane already 24 h after the start of the experiment (48 h from the start of spheroid formation). At the same time, we did not note the transfer of photoconverted microcapsules from mMSCs to EPNT-5.

In general, the migration tracking of individual mMSCs in 2D и 3D EPNT-5 glioblastoma cells colony showed a significant advantage of microcapsules in comparison with the DiD lipophilic membrane dye, which is also used for cell tracking.

 doi:10.20944/preprints202405.1383.v1



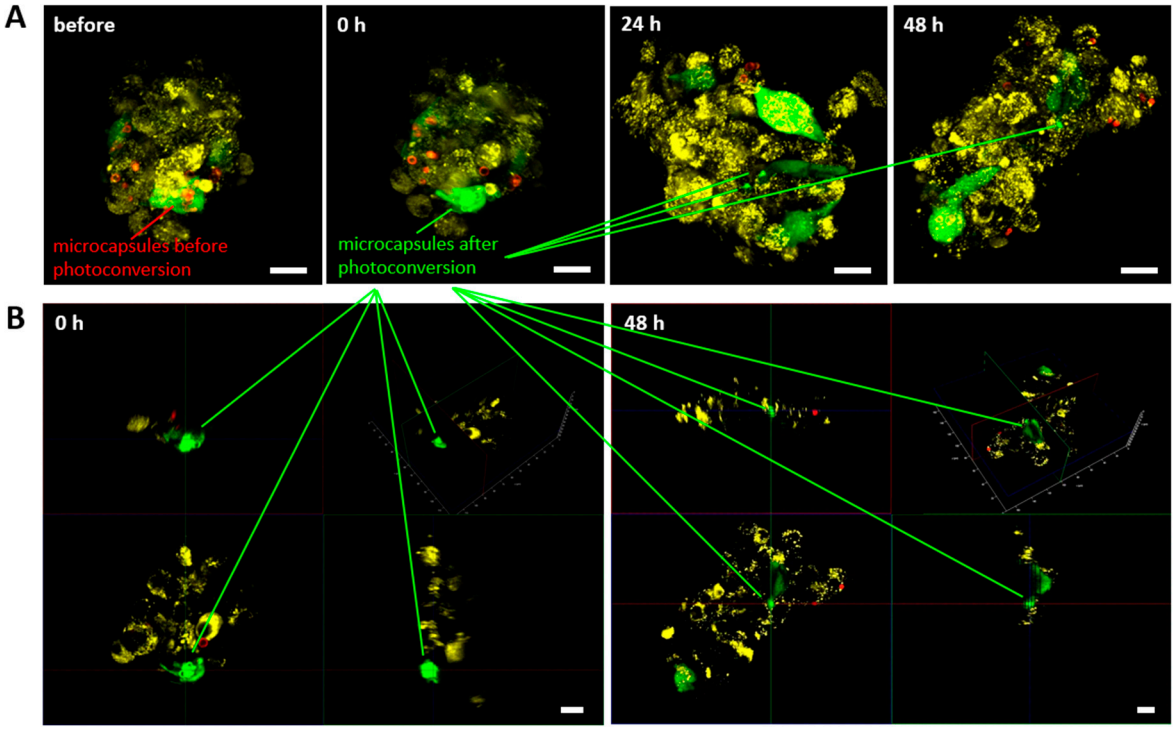


**Figure 6.** (A) Migration of mMSCs (labeled with GFP and photoconverted microcapsules – green) in EPNT-5 glioblastoma cells spheroid (labeled DiD – yellow) at 0, 24, and 48 h. Non-converted capsules – red. (B) 3D reconstruction of EPNT-5 glioblastoma cells spheroid with labeled mMSCs 0 and 48 h after photoconversion. Scale bar – 20 μm.

### *3.5. Detecting of Individual mMSCs Labeled Using Photoconverted Microcapsules in Mouse Brain with Glioblastoma*

The last stage of the study assessed the possibility of identifying labeled mMSCs in solid glioblastoma tumors in mice. For this, the cells were incubated *in vitro* with capsules during 24 h, after which the capsules in individual selected cells were photoconverted (Figure 7A). Next, the mMSCs were detach with trypsin/EDTA solution for 5 min, centrifuged (Figure 7B) and injected in quantity $1 \times 10^6$ in 5 μL DPBS buffer into the mice brain with glioblastoma model at the 21 day after EPNT-5 injection (Figure 7C). 7 days after the animals were injected with 200 μl of 5% Evans Blue solution intravenously. After another 20 minutes, the animals were killed by an overdose of anesthesia. The brain was removed and placed in formalin for further analysis. Note that the introduction of Evans Blue solution made it possible to clearly identify glioblastoma from brain tissue, since this dye does not penetrate cross blood-brain barrier, but penetrate into tumor tissue(Figure 7D).

 doi:10.20944/preprints202405.1383.v1



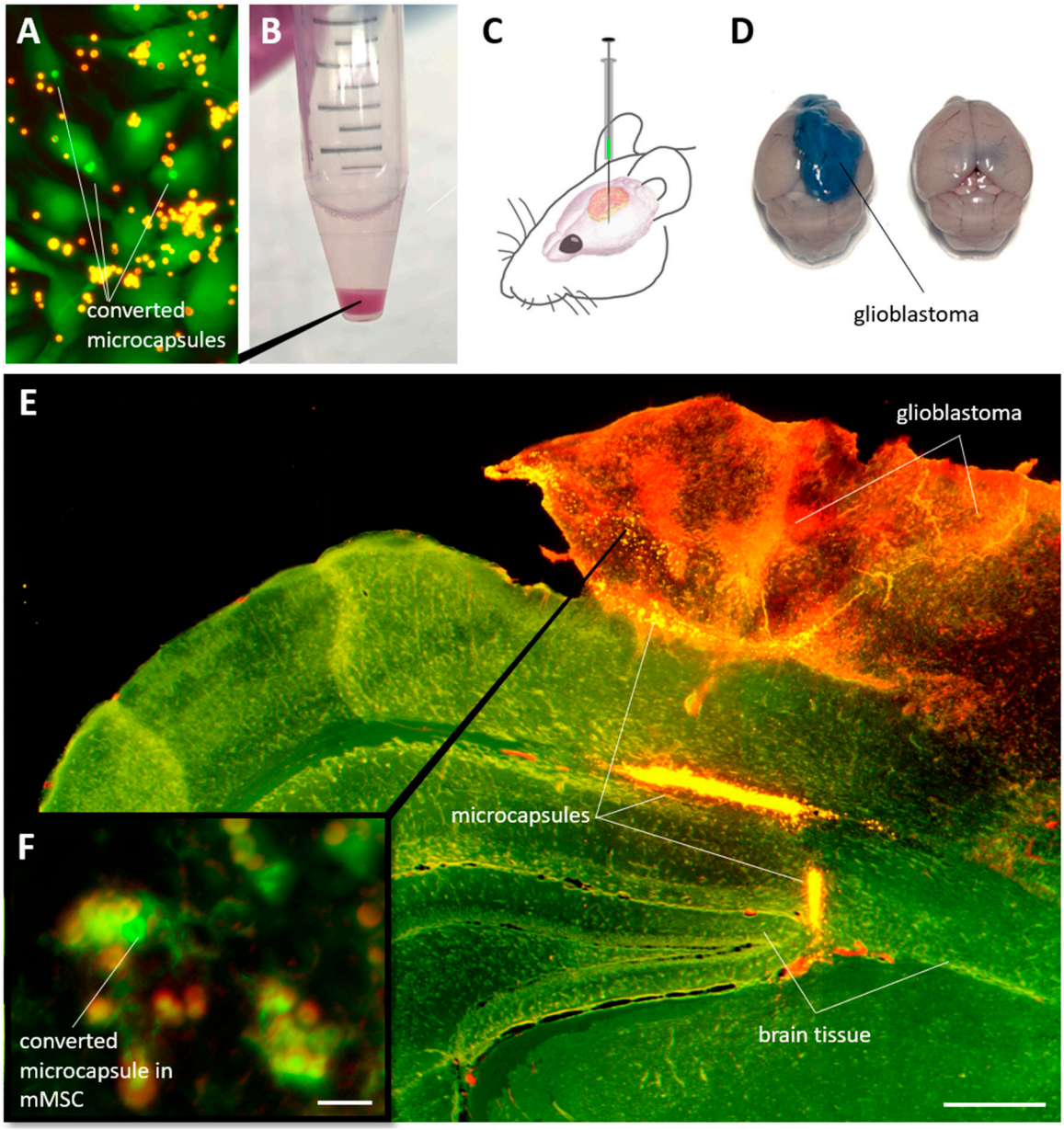


**Figure 7.** (A) Fluorescent images of cells with photoconverted capsules in the cytoplasm. (B) mMSCs containing microcapsules after detaching with trypsin/EDTA solution and centrifugation. (C) The general scheme of mMSCs injection for mouse cells with a glioblastoma model. (D) Mice brain with and without glioblastoma 21d after injection 1 × $10^6$ EPNT-5 cells. The tumor was stained intravitally using an intravenous injection of Evans Blue solution. (E) Fluorescent images of the brain section (green) with glioblastoma (red) and mMSCs contain capsules (yellow). Section thickness – 70 μm. Scale bar – 500 μm. (F) Individually labeled mMSC localized in mouse glioblastoma. Scale bar – 10 μm. .

Analysis of the fluorescent image of brain tissue with glioblastoma showed a bright signal from the capsules, localized mainly at the site of cell injection and along the periphery of the tumor (Figure 7E). A part of the cells were able to penetrate deeper into the tumor, to a depth of approximately 500 μm over 7 days of the experiment. Careful analysis of the sections allowed the identification of individual cells containing photoconverted capsules in their cytoplasm(Figure 7F). Nevertheless, it is worth to note that the search for such cells seems to be a difficult, although possible, task.

In general, these studies have shown that photoconvertible microcapsules are a perspective platform for labeling mMSCs to study their interaction with glioblastoma tumor cells both *in vitro* (in

 doi:10.20944/preprints202405.1383.v1



2D and 3D tumor models) and *in vivo* (in animal models). This is especially important in connection with newly emerging data on the inconsistency of the use of MSCs in oncology therapy. Abundant in vitro or in vivo studies suggest that MSCs increase the number and tumorigenicity of cancer stem cells in varied tumors, including human ovarian tumors [32], breast cancer [33], colorectal tumor [34], prostate cancer [35], Ewing's sarcoma [36], and hepatocellular carcinoma [1] etc. In the same time, MSCs remain in high demand for therapy due to their unique properties: multipotency [37,38], long-term ex vivo proliferation capacity [39,40], self-renewal capacity [41], ability to migrate to tissue injury areas [42], immune modulation [43], and hiding from the immune system [44]. The developed technique could be the key to understanding the complex processes of interaction between MSC and tumor tissue at different stages of oncogenesis and to develop a safe and effective therapeutic strategy.

## 5. Conclusions

The synthesis and characterization of polyelectrolyte fluorescent microcapsules for the effective labeling and tracking of mesenchymal stem cells (MSCs) in both 2D and 3D tumor models, as well as in vivo in a glioblastoma mouse model, are demonstrated in this study. These microcapsules, synthesized with modifications to their surface properties using polymeric layers, were found to exhibit stability and compatibility with cell labeling procedures. Through CLSM, the optimization of photoconversion parameters for achieving maximal fluorescence signal of the labels while minimizing laser exposure, crucial for cellular experiments, was undertaken. Optimal photoconversion was achieved with a one-pixel irradiation duration of 0.4 ms, at a laser power density of 451 kW/cm2 with a wavelength of 561 nm. The vital importance of the selection of the optimal ratio of capsules per cell for effective and safe labeling of MSCs was underscored. Modification of capsules with polyallylamine hydrochloride showed the best potential for intracellular uptake of capsules without significantly affecting viability, motility and proliferation (the ratio of 20 capsules per cell as added to suspension turned out to be optimal). The tracking of the migration of labeled MSCs within glioblastoma cell colonies in both 2D and 3D models revealed the superior performance of microcapsules compared to conventional lipophilic dyes. The ability to reliably identify labeled cells over an extended period without significant signal decay presents a notable advantage for long-term tracking studies. Finally, the potential of photoconvertible microcapsules as a versatile platform for investigating the interactions between MSCs and tumor tissues was demonstrated. The technique developed in this study holds promise for advancing our understanding of MSC-tumor interactions and for facilitating the development of innovative approaches for cancer treatment.

Overall, photoconvertible microcapsules are a promising approach that could be useful for labeling and tracking a wide range of cells in heterogeneous populations. It can also be indispensable for studying the interaction of different cell lines during co-culture, both at the level of the entire population and at the level of individual cells.

**Author Contributions:** Conceptualization, O.A.S.; methodology, O.A.S., P.A.D., Zh.V.K., D.A.T., A.R.M., and O.I.G.; Investigation, O.A.S., P.A.D., Zh.V.K., D.A.T., and O.I.G.; data curation, O.A.S.; writing—original draft preparation, O.A.S., P.A.D., Zh.V.K., D.A.T., and O.I.G.; writing—review and editing, G.B.S.; visualization, O.A.S., P.A.D., Zh.V.K., D.A.T., and O.I.G.; supervision, G.B.S. All authors have read and agreed to the published version of the manuscript.

**Funding:** This research was supported by the Russian Science Foundation (project no. 22-15-00292, https://rscf.ru/prjcard_int?22-15-00292).

**Data Availability Statement:** The data supporting the findings of this study are available from the corresponding author upon reasonable request.

**Acknowledgments:** The authors thank the research center for the collective use of scientific equipment of SSU for their support with confocal microscopy and flow cytometry.

**Conflicts of Interest:** Authors declare no conflict of interest, financial or otherwise.

 doi:10.20944/preprints202405.1383.v1



## Appendix A

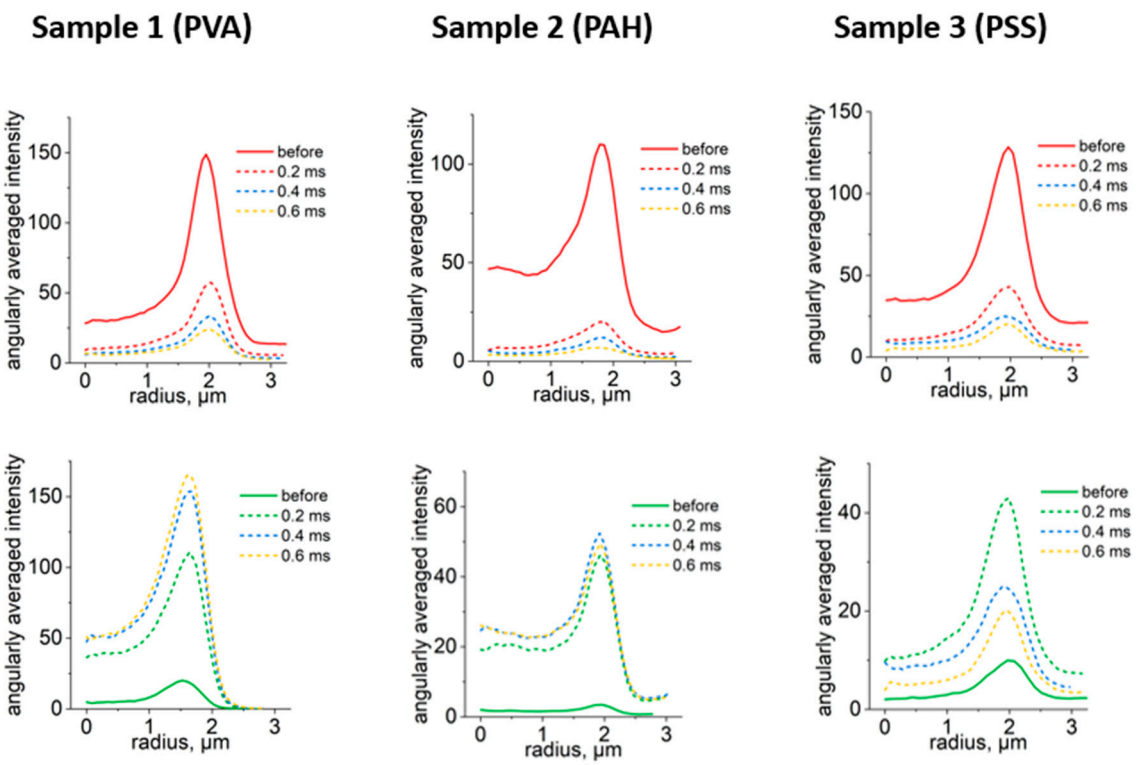


**Figure A1.** Changes in capsules angularly averaged fluorescence intensity profile in green and red channels depending on the duration of one pixel irradiation. Excitation – 488 nm, emission: 505 – 540 nm (green channel), excitation – 561 nm, emission: 580–620 nm (red channel).

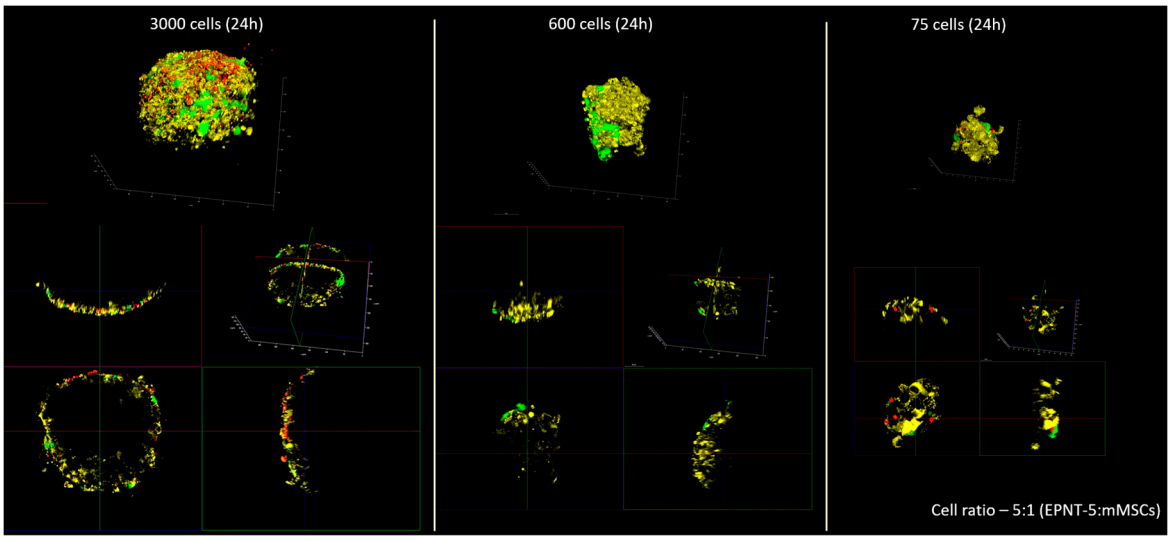


**Figure A2.** Fluorescence images of mMSCs (labeled GFP – green) and EPNT-5 glioblastoma cells spheroid (labeled DiD – yellow) 24 h after placing a mixed cell suspension into the wells of low adhesion 96-well floater plates SDL3D. Non-converted capsules – red.

## References

1. Zhang, X.; Li, N.; Zhu, Y.; Wen, W. The Role of Mesenchymal Stem Cells in the Occurrence, Development, and Therapy of Hepatocellular Carcinoma. *Cancer Med.* **2022**, *11*, 931–943. https://doi.org/10.1002/cam4.4521.

2. Rosu, A.; Ghaemi, B.; Bulte, J.W.M.; Shakeri-Zadeh, A. Tumor-Tropic Trojan Horses: Using Mesenchymal Stem Cells as Cellular Nanotheranostics. *Theranostics* **2024**, *14*, 571–592. https://doi.org/10.7150/thno.90187.
3. Nowakowski, A.; Drela, K.; Rozycka, J.; Janowski, M.; Lukomska, B. Engineered Mesenchymal Stem Cells as an Anti-Cancer Trojan Horse. *Stem Cells Dev.* **2016**, *25*, 1513–1531. https://doi.org/10.1089/scd.2016.0120.
4. Ouyang, X.; Wang, X.; Kraatz, H.-B.; Ahmadi, S.; Gao, J.; Lv, Y.; Sun, X.; Huang, Y. A Trojan Horse Biomimetic Delivery Strategy Using Mesenchymal Stem Cells for PDT/PTT Therapy against Lung Melanoma Metastasis. *Biomater. Sci.* **2020**, *8*, 1160–1170. https://doi.org/10.1039/C9BM01401B.
5. Muslimov, A.R.; Timin, A.S.; Bichaykina, V.R.; Peltek, O.O.; Karpov, T.E.; Dubavik, A.; Nominé, A.; Ghanbaja, J.; Sukhorukov, G.B.; Zyuzin, M. V. Biomimetic Drug Delivery Platforms Based on Mesenchymal Stem Cells Impregnated with Light-Responsive Submicron Sized Carriers. *Biomater. Sci.* **2020**, *8*, 1137–1147. https://doi.org/10.1039/C9BM00926D.
6. Muslimov, A.R.; Timin, A.S.; Petrova, A. V.; Epifanovskaya, O.S.; Shakirova, A.I.; Lepik, K. V.; Gorshkov, A.; Il'inskaja, E. V.; Vasin, A. V.; Afanasyev, B. V.; et al. Mesenchymal Stem Cells Engineering: Microcapsules-Assisted Gene Transfection and Magnetic Cell Separation. *ACS Biomater. Sci. Eng.* **2017**, *3*, 2314–2324. https://doi.org/10.1021/acsbiomaterials.7b00482.
7. Zong, C.; Zhang, H.; Yang, X.; Gao, L.; Hou, J.; Ye, F.; Jiang, J.; Yang, Y.; Li, R.; Han, Z.; et al. The Distinct Roles of Mesenchymal Stem Cells in the Initial and Progressive Stage of Hepatocarcinoma. *Cell Death Dis.* **2018**, *9*, 345. https://doi.org/10.1038/s41419-018-0366-7.
8. Tario Jr., J.D.; Humphrey, K.; Bantly, A.D.; Muirhead, K.A.; Moore, J.S.; Wallace, P.K. Optimized Staining and Proliferation Modeling Methods for Cell Division Monitoring Using Cell Tracking Dyes. *J. Vis. Exp.* **2012**. https://doi.org/10.3791/4287.
9. Lima, C.; Muhamadali, H.; Goodacre, R. Monitoring Phenotype Heterogeneity at the Single-Cell Level within Bacillus Populations Producing Poly-3-Hydroxybutyrate by Label-Free Super-Resolution Infrared Imaging. *Anal. Chem.* **2023**, *95*, 17733–17740. https://doi.org/10.1021/acs.analchem.3c03595.
10. Adam, V.; Moeyaert, B.; David, C.C.; Mizuno, H.; Lelimousin, M.; Dedecker, P.; Ando, R.; Miyawaki, A.; Michiels, J.; Engelborghs, Y.; et al. Rational Design of Photoconvertible and Biphotochromic Fluorescent Proteins for Advanced Microscopy Applications. *Chem. Biol.* **2011**, *18*, 1241–1251. https://doi.org/10.1016/j.chembiol.2011.08.007.
11. Osseiran, S.; Austin, L.A.; Cannon, T.M.; Yan, C.; Langenau, D.M.; Evans, C.L. Longitudinal Monitoring of Cancer Cell Subpopulations in Monolayers, 3D Spheroids, and Xenografts Using the Photoconvertible Dye DiR. *Sci. Rep.* **2019**, *9*, 5713. https://doi.org/10.1038/s41598-019-42165-2.
12. Carlson, A.L.; Fujisaki, J.; Wu, J.; Runnels, J.M.; Turcotte, R.; Celso, C. Lo; Scadden, D.T.; Strom, T.B.; Lin, C.P. Tracking Single Cells in Live Animals Using a Photoconvertible Near-Infrared Cell Membrane Label. *PLoS One* **2013**, *8*, e69257. https://doi.org/10.1371/journal.pone.0069257.
13. Hatta, K.; Tsujii, H.; Omura, T. Cell Tracking Using a Photoconvertible Fluorescent Protein. *Nat. Protoc.* **2006**, *1*, 960–967. https://doi.org/10.1038/nprot.2006.96.
14. Tomura, M.; Ikebuchi, R.; Moriya, T.; Kusumoto, Y. Tracking the Fate and Migration of Cells in Live Animals with Cell-Cycle Indicators and Photoconvertible Proteins. *J. Neurosci. Methods* **2021**, *355*, 109127. https://doi.org/10.1016/j.jneumeth.2021.109127.
15. Caires, H.R.; Gomez-Lazaro, M.; Oliveira, C.M.; Gomes, D.; Mateus, D.D.; Oliveira, C.; Barrias, C.C.; Barbosa, M.A.; Almeida, C.R. Finding and Tracing Human MSC in 3D Microenvironments with the Photoconvertible Protein Dendra2. *Sci. Rep.* **2015**, *5*, 10079. https://doi.org/10.1038/srep10079.
16. Strassburg, S.; Hodson, N.W.; Hill, P.I.; Richardson, S.M.; Hoyland, J.A. Bi-Directional Exchange of Membrane Components Occurs during Co-Culture of Mesenchymal Stem Cells and Nucleus Pulposus Cells. *PLoS One* **2012**, *7*, e33739. https://doi.org/10.1371/journal.pone.0033739.
17. Tomura, M.; Yoshida, N.; Tanaka, J.; Karasawa, S.; Miwa, Y.; Miyawaki, A.; Kanagawa, O. Monitoring Cellular Movement in Vivo with Photoconvertible Fluorescence Protein "Kaede" Transgenic Mice. *Proc. Natl. Acad. Sci.* **2008**, *105*, 10871–10876. https://doi.org/10.1073/pnas.0802278105.
18. Nemet, I.; Ropelewski, P.; Imanishi, Y. Applications of Phototransformable Fluorescent Proteins for Tracking the Dynamics of Cellular Components. *Photochem. Photobiol. Sci.* **2015**, *14*, 1787–1806. https://doi.org/10.1039/c5pp00174a.
19. Demina, P.A.; Sindeeva, O.A.; Abramova, A.M.; Prikhozhdenko, E.S.; Verkhovskii, R.A.; Lengert, E. V.; Sapelkin, A. V.; Goryacheva, I.Y.; Sukhorukov, G.B. Fluorescent Convertible Capsule Coding Systems for Individual Cell Labeling and Tracking. *ACS Appl. Mater. Interfaces* **2021**, *13*, 19701–19709. https://doi.org/10.1021/acsami.1c02767.
20. Demina, P.A.; Sindeeva, O.A.; Abramova, A.M.; Saveleva, M.S.; Sukhorukov, G.B.; Goryacheva, I.Y. Fluorescent Polymer Markers Photoconvertible with a 532 Nm Laser for Individual Cell Labeling. *J. Biophotonics* **2023**, *16*. https://doi.org/10.1002/jbio.202200379.

 doi:10.20944/preprints202405.1383.v1




21. Demina, P.A.; Grishin, O. V.; Malakhov, S.N.; Timaeva, O.I.; Kulikova, E.S.; Pylaev, T.E.; Saveleva, M.S.; Goryacheva, I.Y. Effect of Photoconversion Conditions on the Spectral and Cytotoxic Properties of Photoconvertible Fluorescent Polymer Markers. *Phys. Chem. Chem. Phys.* **2024**, *26*, 13078–13086. https://doi.org/10.1039/D3CP04606K.
22. Kozyreva, Z. V.; Demina, P.A.; Sapach, A.Y.; Terentyeva, D.A.; Gusliakova, O.I.; Abramova, A.M.; Goryacheva, I.Y.; Trushina, D.B.; Sukhorukov, G.B.; Sindeeva, O.A. Multiple Dyes Applications for Fluorescent Convertible Polymer Capsules as Macrophages Tracking Labels. *Heliyon* **2024**, e30680. https://doi.org/10.1016/j.heliyon.2024.e30680.
23. Sindeeva, O.A.; Demina, P.A.; Kozyreva, Z. V.; Muslimov, A.R.; Gusliakova, O.I.; Laushkina, V.O.; Mordovina, E.A.; Tsyupka, D.; Epifanovskaya, O.S.; Sapach, A.Y.; et al. Labeling and Tracking of Individual Human Mesenchymal Stromal Cells Using Photoconvertible Fluorescent Microcapsules. *Int. J. Mol. Sci.* **2023**, *24*, 13665. https://doi.org/10.3390/ijms241713665.
24. Grinchuk, T.M.; Ivantsov, K.M.; Alekseenko, L.L.; Kozhukharova, I. V.; Zaichik, A.M.; Petrov, N.S.; Mikhailov, V.M.; Popov, B. V. Characterizations of the Murine Mesenchymal Cell Line Expressing GFP. *Cell tissue biol.* **2009**, *3*, 29–34. https://doi.org/10.1134/S1990519X09010040.
25. Pinto, B.I.; Cruz, N.D.; Lujan, O.R.; Propper, C.R.; Kellar, R.S. In Vitro Scratch Assay to Demonstrate Effects of Arsenic on Skin Cell Migration. *J. Vis. Exp.* **2019**. https://doi.org/10.3791/58838.
26. Gorin, D.A.; Portnov, S.A.; Inozemtseva, O.A.; Luklinska, Z.; Yashchenok, A.M.; Pavlov, A.M.; Skirtach, A.G.; Möhwald, H.; Sukhorukov, G.B. Magnetic/Gold Nanoparticle Functionalized Biocompatible Microcapsules with Sensitivity to Laser Irradiation. *Phys. Chem. Chem. Phys.* **2008**, *10*, 6899. https://doi.org/10.1039/b809696a.
27. Muñoz Javier, A.; Kreft, O.; Piera Alberola, A.; Kirchner, C.; Zebli, B.; Susha, A.S.; Horn, E.; Kempter, S.; Skirtach, A.G.; Rogach, A.L.; et al. Combined Atomic Force Microscopy and Optical Microscopy Measurements as a Method To Investigate Particle Uptake by Cells. *Small* **2006**, *2*, 394–400. https://doi.org/10.1002/smll.200500282.
28. Merhi, M.; Dombu, C.Y.; Brient, A.; Chang, J.; Platel, A.; Le Curieux, F.; Marzin, D.; Nesslany, F.; Betbeder, D. Study of Serum Interaction with a Cationic Nanoparticle: Implications for in Vitro Endocytosis, Cytotoxicity and Genotoxicity. *Int. J. Pharm.* **2012**, *423*, 37–44. https://doi.org/10.1016/j.ijpharm.2011.07.014.
29. Xiao, K.; Li, Y.; Luo, J.; Lee, J.S.; Xiao, W.; Gonik, A.M.; Agarwal, R.G.; Lam, K.S. The Effect of Surface Charge on in Vivo Biodistribution of PEG-Oligocholic Acid Based Micellar Nanoparticles. *Biomaterials* **2011**, *32*, 3435–3446. https://doi.org/10.1016/j.biomaterials.2011.01.021.
30. Di, J.; Gao, X.; Du, Y.; Zhang, H.; Gao, J.; Zheng, A. Size, Shape, Charge and "Stealthy" Surface: Carrier Properties Affect the Drug Circulation Time in Vivo. *Asian J. Pharm. Sci.* **2021**, *16*, 444–458. https://doi.org/10.1016/j.ajps.2020.07.005.
31. Griswold, S.L.; Sajja, K.C.; Jang, C.; Behringer, R.R. Generation and Characterization of IUBC-KikGR Photoconvertible Transgenic Mice for Live Time-lapse Imaging during Development. *genesis* **2011**, *49*, 591–598. https://doi.org/10.1002/dvg.20718.
32. McLean, K.; Gong, Y.; Choi, Y.; Deng, N.; Yang, K.; Bai, S.; Cabrera, L.; Keller, E.; McCauley, L.; Cho, K.R.; et al. Human Ovarian Carcinoma–Associated Mesenchymal Stem Cells Regulate Cancer Stem Cells and Tumorigenesis via Altered BMP Production. *J. Clin. Invest.* **2011**, *121*, 3206–3219. https://doi.org/10.1172/JCI45273.
33. Liu, S.; Ginestier, C.; Ou, S.J.; Clouthier, S.G.; Patel, S.H.; Monville, F.; Korkaya, H.; Heath, A.; Dutcher, J.; Kleer, C.G.; et al. Breast Cancer Stem Cells Are Regulated by Mesenchymal Stem Cells through Cytokine Networks. *Cancer Res.* **2011**, *71*, 614–624. https://doi.org/10.1158/0008-5472.CAN-10-0538.
34. Ma, X.; Liu, J.; Yang, X.; Fang, K.; Zheng, P.; Liang, X.; Liu, J. Mesenchymal Stem Cells Maintain the Stemness of Colon Cancer Stem Cells via Interleukin-8/Mitogen-Activated Protein Kinase Signaling Pathway. *Exp. Biol. Med.* **2020**, *245*, 562–575. https://doi.org/10.1177/1535370220910690.
35. Luo, J.; Ok Lee, S.; Liang, L.; Huang, C.-K.; Li, L.; Wen, S.; Chang, C. Infiltrating Bone Marrow Mesenchymal Stem Cells Increase Prostate Cancer Stem Cell Population and Metastatic Ability via Secreting Cytokines to Suppress Androgen Receptor Signaling. *Oncogene* **2014**, *33*, 2768–2778. https://doi.org/10.1038/onc.2013.233.
36. Riggi, N.; Suvà, M.-L.; De Vito, C.; Provero, P.; Stehle, J.-C.; Baumer, K.; Cironi, L.; Janiszewska, M.; Petricevic, T.; Suvà, D.; et al. EWS-FLI-1 Modulates MiRNA145 and SOX2 Expression to Initiate Mesenchymal Stem Cell Reprogramming toward Ewing Sarcoma Cancer Stem Cells. *Genes Dev.* **2010**, *24*, 916–932. https://doi.org/10.1101/gad.1899710.
37. Hwang, N.S.; Zhang, C.; Hwang, Y.; Varghese, S. Mesenchymal Stem Cell Differentiation and Roles in Regenerative Medicine. *WIREs Syst. Biol. Med.* **2009**, *1*, 97–106. https://doi.org/10.1002/wsbm.26.
38. Hurley-Novatny, A.; Arumugasaamy, N.; Kimicata, M.; Baker, H.; Mikos, A.G.; Fisher, J.P. Concurrent Multi-Lineage Differentiation of Mesenchymal Stem Cells through Spatial Presentation of Growth Factors. *Biomed. Mater.* **2020**, *15*, 055035. https://doi.org/10.1088/1748-605X/ab9bb0.

39. Fickert, S.; Schröter-Bobsin, U.; Groß, A.-F.; Hempel, U.; Wojciechowski, C.; Rentsch, C.; Corbeil, D.; Günther, K.P. Human Mesenchymal Stem Cell Proliferation and Osteogenic Differentiation during Long-Term Ex Vivo Cultivation Is Not Age Dependent. *J. Bone Miner. Metab.* **2011**, *29*, 224–235. https://doi.org/10.1007/s00774-010-0215-y.
40. Mallis, P.; Michalopoulos, E.; Chatzistamatiou, T.; Giokas, C.S. Interplay between Mesenchymal Stromal Cells and Immune System: Clinical Applications in Immune-Related Diseases. *Explor. Immunol.* **2021**. https://doi.org/10.37349/ei.2021.00010.
41. Sarugaser, R.; Hanoun, L.; Keating, A.; Stanford, W.L.; Davies, J.E. Human Mesenchymal Stem Cells Self-Renew and Differentiate According to a Deterministic Hierarchy. *PLoS One* **2009**, *4*, e6498. https://doi.org/10.1371/journal.pone.0006498.
42. Fu; Liu; Halim; Ju; Luo; Song Mesenchymal Stem Cell Migration and Tissue Repair. *Cells* **2019**, *8*, 784. https://doi.org/10.3390/cells8080784.
43. Müller, L.; Tunger, A.; Wobus, M.; von Bonin, M.; Towers, R.; Bornhäuser, M.; Dazzi, F.; Wehner, R.; Schmitz, M. Immunomodulatory Properties of Mesenchymal Stromal Cells: An Update. *Front. Cell Dev. Biol.* **2021**, *9*. https://doi.org/10.3389/fcell.2021.637725.
44. Mishra, V.K.; Shih, H.-H.; Parveen, F.; Lenzen, D.; Ito, E.; Chan, T.-F.; Ke, L.-Y. Identifying the Therapeutic Significance of Mesenchymal Stem Cells. *Cells* **2020**, *9*, 1145. https://doi.org/10.3390/cells9051145.